Soft Matter

Harnessing biomimetic cryptic bonds to form self-reinforcing gels

Journal:	*Soft Matter*
Manuscript ID	SM-ART-01-2020-000145.R1
Article Type:	Paper
Date Submitted by the Author:	09-Apr-2020
Complete List of Authors:	Biswas, Santidan; University of Pittsburgh, Chemical Engineering Yashin, Victor; University of Pittsburgh, Balazs, Anna; University of Pittsburgh, Chemical Engineering

Harnessing biomimetic cryptic bonds to form self-reinforcing gels

Santidan Biswas, Victor V. Yashin, Anna C. Balazs*

Chemical Engineering Department, University of Pittsburgh, Pittsburgh, PA 15261,

United States

* balazs@pitt.edu

Abstract

Cryptic sites, which lay hidden in folded biomolecules, become exposed by applied force and form new bonds that reinforce the biomaterial. While these binding interactions effectively inhibit mechanical deformation, there are few synthetic materials that harness mechano-responsive cryptic sites to forestall damage. Here, we develop a computational model to design polymer gels encompassing cryptic sites and a lower critical solution temperature (LCST). LCST gels swell with a decrease in temperature, thereby generating internal stresses within the sample. The gels also encompass loops held together by the cryptic sites, as well as dangling chains with chemically reactive ends. A decrease in temperature or an applied force causes the loops to unfold and expose the cryptic sites, which then bind to the dangling chains. We show that these binding interactions act as "struts" that reinforce the network, as indicated by a significant decrease in the volume of the gel (from 44% to 80%) and shifts in volume phase transition temperature. Once the temperature is increased or the deformation is removed, the latter "cryptic bonds" are broken, allowing the loops to refold and the gel to return its original state. These findings provide guidelines for designing polymer networks with reversible, mechano-responsive bonds, which allow gels to undergo a self-stiffening behavior in response to a temperature-induced internal stress or external

force. Applied as a coating, these gels can prevent the underlying materials from undergoing damage and thus, extend the lifetime of the system.

I. Introduction

Biological systems display a variety of mechanisms to mitigate the effects of an applied force, and even harness the force to perform a useful function. For example, when prodded or poked, the armadillo curls up into a ball, so that its dermal armor protects it from further harm. The Venus fly trap snaps shut when insects exert a force on its leaves, and thus, the plant consumes its prey. The exposure of cryptic binding sites is another prime example of an adaptive, biological response to mechanical force that ultimately produces the beneficial effect of strengthening the biomaterial. Cryptic binding sites[1] lie buried and hidden within folded biopolymers (e.g., proteins), but are uncovered under a mechanical deformation. The exposed cryptic sites then participate in bond formation, which in turn leads to more interconnected and stronger structures. Such cryptic binding sites play a crucial role in the structure formation of fibronectin (Fn), which is essential for wound healing, [2] embryonic development, and normal functioning of vertebrates. [3]

Despite their utility in soft biomaterials, there have been few studies on utilizing the combination of mechanical deformation and cryptic binding sites to tailor the behavior of soft synthetic materials, such as polymer gels.[4–6] Incorporated into a polymer network, cryptic sites could provide a number of distinct advantages, which are best illustrated by referring to the schematic in Fig. 1. The green polymer network contains loops that are held together by a "cryptic bond", which is formed between the blue cryptic sites. From a mechanics point of view, such loops are essentially "wasted" since they do not improve the strength or toughness of the material.[7] The application of force breaks the cryptic bonds and frees the "hidden length" that was stored in the

loops. Exposed in this way, the cryptic binding sites and the hidden length can now both contribute to improving the mechanical properties of the network.

As is typical in polymer gels, the network in Fig. 1 also contains dangling chains that branch off the main framework. These dangling chains encompass reactive end groups, which are marked in yellow within the figure. Similar to the wasted loops, the unbound dangling ends do not contribute to optimizing the material's mechanical performance. If, however, the reactive ends bind to the exposed cryptic sites, they could form "struts" that stiffen the gel. This mechano-responsive stiffening would allow the material to resist further deformation (up to some critical level) and thus, extend the functionality of the gel. In other words, the introduction of the mechano-responsive cryptic sites provides a means of improving the materials' mechanical properties in the presence of an applied force (or other external stimulus).

Herein, we model the complex dynamics involving the unfolding of the loops and subsequent binding (and unbinding) of dangling ends to the exposed binding sites (Fig. 1). Using this model, we determine factors that affect these reversible processes and demonstrate the self-stiffening of the gel. The gel in our system is taken to be poly(N-isopropylacrylamide) (pNIPAAm), which exhibits a lower critical solution temperature (LCST). Hence, the gel shrinks above the volume phase transition temperature (T_c), which is approximately $33°C$ for pNIPAAm, and swells in volume as the temperature is lowered below T_c. With the introduction of these structural features (Fig.1), we find a substantive decrease in the degree of swelling of the LCST gel below T_c. Namely when the temperature is lowered to $31.5°C$, the volume of gels considered here can be 44% lower than that of gels that do not undergo the binding interactions shown in Fig. 1. This decrease in swelling occurs because the loops unfold and the newly available binding sites form bonds with the dangling ends. Hence, the system exhibits an increase in cross-link density

and a self-stiffening behavior. We also show that this self-stiffening can take place at fixed temperatures when the gel is deformed by a constant applied force. In particular at 34.5°C, the volume of uniaxially stretched gels that include binding interactions between the exposed cryptic sites and dangling ends can be approximately 80% lower than that for the gels without this binding. Under these circumstances, the force-induced self-reinforcement effectively enables the gel to resist further mechanical deformation.

Through these studies, we devise a powerful approach for creating self-stiffening or self-reinforcing materials that dynamically form a "dermal armor" to protect the underlying system from damage. Namely, by harnessing the mechano-responsive behavior of bio-inspired cryptic bonds, we can design materials that provide a beneficial response to mechanical deformation. Applied as a coating, such responsive self-forming armor can enhance the durability of everyday objects and surfaces.

II. Methodology

A. Theoretical model

Herein, we augment our recently developed model[5] of a permanently cross-linked, swollen polymer gel that encompasses loops by introducing end-functionalized dangling chains that are attached to the network. *Via* this augmented model, we can determine new mechanisms for creating self-reinforcing polymer gels. As shown in Fig. 1, the ends of the dangling chains are capped by yellow reactive sites; the grey disks represent the permanent cross-links in the network. The chains in green are subchains between these permanent cross-links. Some subchains contain two reactive "cryptic" sites, which can bind to each other (blue circles in Fig. 1) through a labile, reformable bond, and thus form a loop in the subchain, or remain unbound (red circles). These red species mimic the exposed cryptic binding sites in fibronectin[1,4] that can bind with adjacent linkers and

thereby stiffen the network. In our system, the unbound ("exposed") cryptic sites can form a reversible bond with the yellow ends on the dangling chains.

In the undeformed state (i.e., the state of the gel as fabricated), some cryptic sites are bound to each other to form loops in the subchains, some loops are open, and a fraction of the exposed cryptic sites are bound to the reactive ends of the dangling chains (as drawn in Fig. 1). Upon deformation, labile bonds between loop-forming cryptic sites are broken, causing the loop to unfold. In this unfolded state, the exposed cryptic sites can form temporary cross-links with the reactive ends of the dangling chains. If the deformation is released, then some labile bonds forming the temporary cross-links will break, and the cryptic sites can reform the loops, so that the subchains return to their initial configuration. For simplicity, we assume that all loops are closed in the as-fabricated gel.

Every subchain in the network contains $n+l$ Kuhn segments; for subchains containing loops, the l segments lie within the loop. The dangling chains contain m Kuhn segments, as shown in Fig. 1. To formulate the equations that describe the kinetics of binding and unbinding in the polymer network, we assume that the time scale for the breaking and reforming of a bond between the reactive groups is longer than the time scale associated with the conformational changes of the chain. In this case, the binding and unbinding can be described by equations for the chemical kinetics in the network.

We start by introducing the necessary notation and simplifying assumptions. The concentrations of the subchains encompassing the loops and dangling chains are denoted as c_l and c_d, respectively. The total concentration of the exposed cryptic sites is $n_c = 2p_U c_l$, where p_U is the fraction of subchains with unfolded loops. The fraction of exposed cryptic sites that are bound to the dangling chains is denoted π_B, so that the concentration of the latter sites is $n_c^{(b)} = \pi_B n_c$.

We assume that there are two dangling chains per subchain and hence, the total concentration of the reactive end-units is $n_d = 2c_d$, and the concentration of end-units and hence, dangling chains bound to the cryptic sites is $c^* = p_B n_d$, where p_B is the fraction of bound dangling chains. Note that, $n_c^{(b)} = c^*$ and, therefore, $\pi_B p_U c_l = p_B c_d$. Finally, we assume that the network contains equal amounts of the subchains encompassing the loops and dangling chains, and that no other type of subchains is present in the network; therefore, $c_l = c_d = 2^{-1}\phi_0^{-1}\phi c_0$. Here, c_0 and ϕ_0 are the respective concentrations of polymer strands and the volume fraction of polymer in the undeformed network, and ϕ is the volume fraction of polymer in the actual state of the system. It is worth noting that in the theory of rubber elasticity, the cross-link density, c_0, (by definition) characterizes the undeformed sample. The value $c^* = \phi_0^{-1}\phi c_0 p_B$ is hence interpreted as the density of temporary cross-links.

The fraction of unfolded loops, p_U, as a function of time t is described by the following rate equation:

$$dp_U/dt = k_r(1-p_U) - k_f(1-\pi_B)^2 p_U \quad , \qquad (1)$$

where, k_r and k_f are the respective rate constants for the rupture and formation of the labile bond between the two cryptic sites. The values of k_r and k_f depend on the distance between the subchain ends that form the loop, as discussed in detail below. Equation (1) is a modification of the relevant equation in our previously developed model for polymer chains with loops[5] ; the new equation accounts for inhibition of the folding process due to the binding of the dangling chains to the exposed cryptic sites. The factor $(1-\pi_B)^2$ in the second term on the right-hand side of eq. (1) is the probability that both exposed cryptic sites in a subchain are unbound, so subsequent loop

formation could occur. For simplicity, eq. (1) neglects the formation of labile bonds between the exposed cryptic sites belonging to different subchains.

When the loops unfold, the end-groups of the dangling chains could bind to the exposed cryptic sites (Fig. 1). The density of temporary cross-links, c^*, is determined by a competition between the binding and un-binding events, which are controlled by the respective rate constants, K_{compl} and K_{uB}, for the complexation and un-binding :

$$dc^*/dt = K_{compl}(n_c - n_c^{(b)})(n_d - c^*) - K_{uB}\,c^* \quad .$$

The reaction rate constants K_{compl} and K_{uB} depend on the network structure and state of deformation, as described in detail below. It is useful to rewrite the above rate equation in terms of the fraction of bound dangling chains, p_B, using the notation and simplifying assumptions discussed above:

$$dp_B/dt = \phi_0^{-1}\phi\, c_0\, K_{compl}\, p_U(1-\pi_B)(1-p_B) - K_{uB}p_B \quad . \qquad (2)$$

At a constant degree of swelling, ϕ is a constant; eqs. (1) and (2) form a closed set of equations for the values p_U and p_B because the fraction of cryptic sites bound to the dangling chains, π_B, is not an independent variable since, as discussed above, $p_B = \pi_B p_U$.

The rate constants for the rupture and formation of labile bonds between the cryptic sites, k_r and k_f, respectively, are calculated as in our previous study.[5] We take into account that stretching a subchain encompassing a closed loop increases the force acting on the labile bond connecting the two cryptic sites and hence, facilitates bond rupture. We utilize the Bell model[8] to calculate the rupture rate constant as a function of the distance between the chain ends, R :

$$k_r(R) = k_r^{(0)}\exp[\gamma_{0R}\,F_n(R)/k_BT] \quad . \qquad (3)$$

Here, $k_r^{(0)}$ is the rupture rate at zero force, $F_n(R)$ is the force needed to separate the ends of a chain of n segments to the distance R, and γ_{0R} is the parameter that characterizes the sensitivity of the bond to the applied force, and k_B and T are the respective Boltzmann's constant and temperature. The loop does not contribute to $F_n(R)$, which depends only on the number of segments n in the unlooped part of the chain (Fig. 1). The force acting on the bond when the chains are stretched is calculated according to the freely-jointed chain model (FJC),[9] which accounts for the finite extensibility of the chain and yields the following expression:

$$F_n(R) = \frac{k_B T}{b} \mathcal{L}^{-1}[R(nb)^{-1}] \ , \tag{4}$$

where

$$\mathcal{L}(x) = \coth(x) - x^{-1} \tag{5}$$

is the Langevin function, and b is the length of the Kuhn segment. We take into account the finite chain extensibility because it has a strong effect on the rate of bond rupture, i.e., through the expression for $F_n(R)$ in eq. (3).

The rate constant for forming a labile bond, $k_f(R)$, depends on the chain end-to-end distance R because to form a bond, the reactive units in the unfolded chain of $n+l$ segments must first come into contact, and the probability of contact, P_c, depends on R. When in contact, the reactive units form a labile bond with the rate constant $k_f^{(0)}$, and hence $k_f(R) = P_c(R) k_f^{(0)}$. As in previous studies[10–14], it is assumed that $k_f^{(0)}$ does not depend on the force acting on the bond. The probability of contact, $P_c(R)$, is calculated using the conformational statistics of the polymer chain: $P_c(R) = P_n(R) P_l(0) / P_{n+l}(R)$, where $P_n(R)$ is the probability distribution function for

finding the ends of a chain of n segments at distance R apart. For the FJC model, this distribution function is [9]

$$P_n(R) = \frac{[\mathcal{L}^{-1}(x)]^2}{(2\pi nb^2)^{3/2} x \{1-[\mathcal{L}^{-1}(x)\operatorname{csch}(\mathcal{L}^{-1}(x))]^2\}^{1/2}} \left[\frac{\sinh \mathcal{L}^{-1}(x)}{\mathcal{L}^{-1}(x)}\right]^n \exp[-nx\mathcal{L}^{-1}(x)] \quad (6)$$

where $x = R(nb)^{-1}$. Note that through the equations for $P_c(R)$, the rate of chain folding depends on both the total length of the chain, $n+l$, and the length of the loop, l.

It is convenient to re-write the dimensionless variable $x = R(nb)^{-1}$ in eqs. (5) and (6) in terms of the chain extension λ. It is worth recalling that we assume that all the loops are folded when the gel is in the undeformed state. Given that b is the length of one segment, the average end-to-end distance of an unperturbed chain is thus $R_0 = b\sqrt{n}$, since l segments are part of the closed loop. At a given chain extension λ, the end-to-end distance R of a deformed chain with a closed loop is calculated as $R = \lambda R_0$ and hence, $x = \lambda n^{-1/2}$ in eqs. (5) and (6). This allows us to consider the rate constants of bond rupture and formation as functions of λ instead of that of R, i.e., $k_r(\lambda)$ and $k_f(\lambda)$, respectively.

The rate constant for complex formation in eq. (2), K_{compl}, is proportional to the probability that the two reacting monomeric units will meet. We employ the approach by Ito, *et al.*,[15] to account for the restrictions imposed by the polymer network on the binding of the dangling chains to the exposed cryptic sites. According to ref. [15], the restrictions on the motion of a reacting unit grafted to a subchain are captured by assuming that the reactive unit is attached to one end of a fictitious Gaussian chain, whose length is half of the subchain length. The other end of this fictitious chain is fixed in space. When the two reacting units meet, the two fictitious chains form a chain connecting the two fixed points. The probability for the two reacting units to meet is taken to be proportional to the Boltzmann factor associated with the loss of entropy due to the formation

of the polymer chain, whose end-to-end distance is equal to the average spatial separation between the reacting units.[15] Correspondingly, we calculate K_{compl} as

$$K_{compl} = K_0 \exp(-\rho^2 / Nb^2) \quad , \tag{7}$$

where K_0 includes the chemical factors affecting the complexation, and the exponential term describes the entropy restrictions associated with the complex formation. In eq. (7), ρ is the characteristic distance between the reacting units, N is the number of Kuhn segments in the fictitious Gaussian chain, and b is the Kuhn length. The distance ρ is determined as $\rho = c_0^{-1/3}(\phi / \phi_0)^{-1/3}$, because the concentration of dangling chains is $n_d = 2c_d = c_0\phi_0^{-1}\phi$ (see above), so the characteristic distance between an exposed cryptic site and end of a dangling chain is $\rho = n_d^{-1/3}$. The number of segments in the newly formed fictitious chain is $N = n + m + l$, since the chain consists of a half of the subchain encompassing the dangling chain, the dangling chain itself, and a half of the subchain encompassing the exposed cryptic bond. Note that the values ϕ_0 and c_0 are related to each other as

$$\phi_0 = c_0 a_0^2 b (n + m + l) \quad , \tag{8}$$

where a_0 is the size of a monomeric unit so $a_0^2 b$ is the volume of Kuhn segment. As a result, we obtain the following equation for the complexation rate constant as a function of the volume fraction of polymer ϕ:

$$K_{compl}(\phi) = K_0 \exp[-(a_0 / b)^{4/3}(n + m + l)^{-1/3}\phi^{-2/3}] \tag{9}$$

Finally, the rate constant for the unbinding of a dangling chain in eq. (2), K_{uB}, is calculated as a function of the chain extension λ using the Bell model to obtain an equation similar to eq. (3):

$$K_{uB}(\lambda) = k_{uB}^{(0)} \exp[\gamma_{uB} F_m(\lambda) / k_B T] \quad . \tag{10}$$

Here, $F_m(\lambda) = \frac{k_B T}{b} \mathcal{L}^{-1}[\lambda m^{-1/2}]$ is the force acting on a chain consisting of m segments under an extension λ (cf. eq. (4)), and $k_{uB}^{(0)}$ and γ_{uB} are the respective reaction rate constant at zero force and the force sensitivity parameter.

B. Modeling the dynamic response of the gel to deformation

To describe the dynamic behavior of the material under deformation, we extend our previously developed gel lattice-spring model (gLSM) computational approach [16–18] to incorporate the effects of binding the dangling chains to exposed cryptic sites. For this purpose, we first specify the energy density of a deformed material, $u(I_1, I_3)$, as a function of the invariants I_1 and I_3 of the Finger strain tensor, $\hat{\mathbf{B}}$. The gLSM equations used in the simulations are determined through a finite-element approximation of the energy density, as described below.

The total energy, $U_{tot} = v_0^{-1} k_B T \int u(I_1, I_3) dV_0$, is determined through integration over the volume of the unstrained material, V_0. Here, $v_0 = a_0^3$ is the volume of a monomeric unit and the factor $v_0^{-1} k_B T$ is the unit of stress in our model. For the gel model considered here, the energy density is dimensionless and is composed of three terms:

$$u(I_1, I_3) = u_{\mathrm{el}}(I_1, I_3) + u_{\mathrm{FH}}(I_3) + u_{\mathrm{el}}^{*}(t) \quad . \tag{11}$$

The first term on the right-hand side (r.h.s.) of eq. (11), $u_{\mathrm{el}}(I_1, I_3)$, describes the elastic energy of the crosslinked network within the approximation of affine deformations

$$\begin{aligned} u_{\mathrm{el}}(I_1, I_3) = {} & \frac{c_0 v_0}{2} \Big[(1 - p_U) \Psi(I_1, n) + p_U \Psi(I_1, n(1 + l/n)^2) + \Psi(I_1, n + l) \Big] \\ & - \frac{c_0 v_0}{4} \big[\zeta_0(n) + \zeta_0(n + l) \big] \ln I_3^{1/2} \end{aligned} \quad . \tag{12}$$

Here, c_0 is the total concentration of subchains in the as-prepared gel. The function $\Psi(I_1, n_{\rm el})$ is defined as

$$\Psi(I_1, n_{\rm el}) = n_{\rm el}\left[\psi\left(\sqrt{\frac{I_1}{3n_{\rm el}}}\right) - \psi(n_{\rm el}^{-1/2})\right] \qquad (13)$$

and gives the contribution of a stretched FJC chain consisting of $n_{\rm el}$ elastically active segments to the elastic energy. In eq. (13), the function $\psi(x)$ in an antiderivative of the inverse Langevin function

$$\psi(x) = x\mathcal{L}^{-1}(x) + \ln\left(\frac{\mathcal{L}^{-1}(x)}{\sinh[\mathcal{L}^{-1}(x)]}\right) \quad .$$

It is also convenient to introduce the function $\zeta(x)$ defined as

$$\zeta(x) = (3x)^{-1}\mathcal{L}^{-1}(x) \quad .$$

Finally, $\zeta_0(n) = \zeta(n^{-1/2})$ in eq. (12).

Equation (12) is a generalization of the neo-Hookean elastic energy to the case of permanently cross-linked FJC chains. [19] The first term on the r.h.s. of eq. (12) describes the the entropic elasticity of stretched polymer chains, and the second term is the contribution of the ideal gas of permanent crosslink points.

As noted previously, all the subchains between the cross-links are assumed to have $n + l$ segments. One half of the subchains contain a loop, and the loops are assumed to be folded in the un-deformed gel. In eq. (12), the first two contributions to the entropic elasticity term account for the subchain configurations having the folded and unfolded loops, for which $n_{\rm el} = n$ and $n_{\rm el} = n(1 + l/n)^2$, respectively. The number of elastically active segments for the unfolded configuration is taken to be equal to the effective number $n_{\rm el} = n(1 + l/n)^2$ because in the

calculations of the rate of folding, the subchains with folded and unfolded loops are considered to have the same end-to-end distances. The third contribution to the entropic elasticity term in eq. (12) describes the subchains that contain dangling chains and for which $n_{\mathrm{el}} = n + l$. The entropic elasticity contribution of the dangling chains bound to the exposed cryptic bonds is taken into account separately and is discussed further below.

The second term on the r.h.s. of eq. (11) describes the polymer-solvent interaction according to the Flory-Huggins model

$$u_{\mathrm{FH}}(I_3) = I_3^{1/2}\left[(1-\phi)\ln(1-\phi) + \chi_{FH}(\phi,T)\phi(1-\phi)\right] \tag{14}$$

In eq. (14), the volume fraction of polymer ϕ itself depends on I_3 as $\phi = \phi_0 I_3^{-1/2}$, where ϕ_0 is the volume fraction of polymer in the un-deformed state, and $\chi_{FH}(\phi,T)$ is the Flory-Huggins interaction parameter.

The dangling chains contribute to the elastic energy only when they form temporary cross-links by attaching to the exposed cryptic bonds. The contribution of the temporary cross-links is described by the last term on the r.h.s. of eq. (11) and has the following form:

$$\begin{aligned} u^*_{\mathrm{el}}(t) = {} & c_0^* v_0 \xi(t,0)\left[\Psi(I_1(t,0),m) - \frac{\zeta_0(m)}{2}\ln(I_3^{1/2}(t,0))\right] \\ & + c_0^* v_0 \int_0^t \frac{\partial \xi}{\partial \tau}(t,\tau)\left[\Psi(I_1(t,\tau),m) - \frac{\zeta_0(m)}{2}\ln(I_3^{1/2}(t,\tau))\right] d\tau \end{aligned} \tag{15}$$

Equation (15) is the generalization of eq. (12) to the case of transient networks, where deformations at a given time are affected by deformations that occurred earlier in the sample.[20,21] Specifically, the stress tensor within a transient network depends on the relative strain tensor $\hat{\mathbf{b}}(t,\tau)$, which characterizes deformations in the network at time *t* relative to the (deformed) state of the network at τ. Correspondingly, $u^*_{\mathrm{el}}(t)$ depends on the invariants of the relative strain tensor $I_1(t,\tau)$ and

$I_3(t,\tau)$.[21] It is worth noting that $\hat{\mathbf{b}}(t,0)=\hat{\mathbf{B}}(t)$. We calculate $\bar{\lambda}(t,\tau)$ by averaging the relative principal strains, namely, $\bar{\lambda}(t,\tau)=3^{-1/2}\sqrt{\sum_{i=1}^{3}\lambda_i^2(t)\,\lambda_i^{-2}(\tau)}$, where $\lambda_i(\tau)$ and $\lambda_i(t)$, $i=1,2,3$, are the principal strains calculated at the moments of time τ and t, respectively.

The function $\xi(t,\tau)$ on the r.h.s. of eq. (15) determines the number of cross-links that were created before the time τ and still exist at time $t\geq\tau$. The time derivative $\partial\xi(t,\tau)/\partial\tau$ determines the number of cross-links that exist at time t and were created during the period of time from τ to $\tau+d\tau$. To specify the functions $\xi(t,0)$ and $\partial\xi(t,\tau)/\partial\tau$, we write the formal solution of eq. (2) for the fraction of bound dangling chains p_B:

$$p_B(t)=p_B(0)\exp[-\int_0^t K_{uB}(\tau,0)d\tau]+\int_0^t\exp[-\int_\tau^t K_{uB}(\tau',\tau)\,d\tau']K_B(\tau)d\tau \quad . \tag{16}$$

In the above equation, the rate of binding $K_B(t)$ is defined as

$$K_B=c_0\phi_0^{-1}\phi\,K_{compl}(\phi)(1-p_B)(p_U-p_B) \quad , \tag{17}$$

and depends on time t through the time-dependent fractions of unfolded loops, p_U, and bound dangling chains, p_B, and the time-dependent volume fraction of polymer ϕ. Correspondingly, the functions $\xi(t,0)$ and $\partial\xi(t,\tau)/\partial\tau$ on the r.h.s. of eq. (15) are calculated as

$$\xi(t,0)=p_B(0)\exp[-\int_0^t K_{uB}(\tau,0)d\tau] \quad , \tag{18}$$

$$\frac{\partial\xi}{\partial\tau}(t,\tau)=\exp[-\int_\tau^t K_{uB}(\tau',\tau)\,d\tau']K_B(\tau) \quad . \tag{19}$$

The rate constant of unbinding $K_{uB}(t,\tau)$ in eqs. (18) and (19) is calculated according to eq. (10), and depends on both the time t and the time of bond creation $\tau \le t$. The latter dependence arises because a newly formed cross-link experiences no force at the moment of creation τ, and the force acting on it at the time t depends on the relative chain extension $\lambda(t,\tau)$.

After specifying the energy density, the constitutive equation, which provides the stress-strain relationships in the material, is readily formulated[21] to obtain the following equation for the stress tensor $\hat{\boldsymbol{\sigma}}$:

$$\hat{\boldsymbol{\sigma}} = \hat{\boldsymbol{\sigma}}_{\mathrm{el}} - \pi_{\mathrm{FH}}(\phi,T)\hat{\mathbf{I}} + \hat{\boldsymbol{\sigma}}^{*}_{\mathrm{el}}(t) \quad , \tag{20}$$

where $\hat{\mathbf{I}}$ is the unit tensor. In eq. (20), $\hat{\boldsymbol{\sigma}}_{\mathrm{el}}$ is the elastic stress due to the FJC chains

$$\begin{aligned}\hat{\boldsymbol{\sigma}}_{el} = \frac{c_0 v_0}{2}\left[(1-p_U)\,\zeta\left(\frac{\bar{\lambda}}{\sqrt{n}}\right) + p_U\,\zeta\left(\frac{\bar{\lambda}\sqrt{n}}{n+l}\right) + \zeta\left(\frac{\bar{\lambda}}{\sqrt{n+l}}\right)\right]\frac{\phi}{\phi_0}\hat{\mathbf{B}} \\ - c_0 v_0[\zeta_0(n)+\zeta_0(n+l)]\frac{\phi}{4\phi_0}\hat{\mathbf{I}}\end{aligned} \quad , \tag{21}$$

and $\pi_{\mathrm{FH}}(\phi,T)$ is the osmotic pressure of the polymer in the system according to the Flory-Huggins model

$$\pi_{\mathrm{FH}}(\phi,T) = -[\phi + \log(1-\phi) + \chi(\phi,T)\phi^2] \quad . \tag{22}$$

Finally, $\hat{\boldsymbol{\sigma}}^{*}_{\mathrm{el}}(t)$ is the elastic stress due to the temporary cross-links

$$\begin{aligned}\hat{\boldsymbol{\sigma}}^{*}_{\mathrm{el}}(t) = c_0^{*} v_0 \xi(t,0)\frac{\phi}{\phi_0}\left[\zeta\left(\frac{\bar{\lambda}(t,0)}{\sqrt{m}}\right)\hat{\mathbf{b}}(t,0) - \frac{\zeta_0(m)}{2}\hat{\mathbf{I}}\right] + \\ + c_0^{*} v_0 \frac{\phi}{\phi_0}\int_0^t \frac{\partial \xi}{\partial \tau}(t,\tau)\left[\zeta\left(\frac{\bar{\lambda}(t,\tau)}{\sqrt{m}}\right)\hat{\mathbf{b}}(t,\tau) - \frac{\zeta_0(m)}{2}\hat{\mathbf{I}}\right]d\tau\end{aligned} \tag{23}$$

In eq. (22), the interaction parameter $\chi(\phi,T)$ is related to the Flory-Huggins interaction parameter $\chi_{FH}(\phi,T)$ in eq. (14) as $\chi(\phi,T)=\chi_{FH}(\phi,T)+(1-\phi)\partial_{\phi}\chi_{FH}(\phi,T)$. All other notations are the same as introduced before.

The equilibrium swelling of a gel that contains both cryptic bonds and dangling binding chains is determined by solving of eqs. (1), (2), and (20) in the steady-state limit, i.e., by solving the system of equations $dp_U/dt=0$, $dp_B/dt=0$, and $\hat{\boldsymbol{\sigma}}=\mathbf{0}$. In order to determine the equilibrium value of $\hat{\boldsymbol{\sigma}}^{*}_{\mathrm{el}}$, we note that $\xi(t,0)\to 0$ at $t\to\infty$, and that $\hat{\mathbf{b}}(t,\tau)=\hat{\mathbf{I}}$ and $\bar{\lambda}(t,\tau)=1$ at equilibrium. According to eqs. (16), (18), and (19), the probability of binding can be calculated as $p_B(t)=\xi(t,0)+\int_0^t\frac{\partial\xi}{\partial\tau}(t,\tau)d\tau$. Then, the following equilibrium limit of eq.(23) is found:

$$\hat{\boldsymbol{\sigma}}^{*}_{\mathrm{el}}=p_B c_0^{*} v_0\phi(2\phi_0)^{-1}\zeta_0(m)\hat{\mathbf{I}} \quad . \tag{24}$$

The equilibrium value rate constant of unbinding K_{uB}, eq. (10), should be calculated at the chain extension $\bar{\lambda}=1$, because K_{uB} depends on the relative strain.

C. Computational model

The 3D gel lattice spring model (gLSM) computational technique[16–18] allows to numerically solve the above analytical equations and thus simulate the dynamic behavior of the gels with loops and dangling chains with reactive ends. The combination of finite element and finite difference approaches at the core of the gLSM provides an effective method to numerically solve the elastodynamic equations characterizing the behavior of chemo-responsive polymer gels. The gLSM was initially developed to simulate the dynamic behavior of self-oscillating polymer gels undergoing the Belousov-Zhabotinsky (BZ) reaction [16–18,22,23] and to predict the response of these BZ gels to an applied force.[24–27] For instance, we focused on a BZ gel confined in a capillary

tube and determined the effect of applying a compressive force P to the confined ends. Our computer simulations revealed that upon introduction of chemo-responsive crosslinks to the polymer network, the compression of the BZ gel leads to an increase in the cross-link density within the sample and thus, a stiffening of the gel.[26] Subsequent experimental studies[27,28] validated the predictions that emerged from these computational studies. We later modified the gLSM to account for the formation of additional, reversible cross-links due to changes in the degree of oxidation of polyacrylamide-based BZ gels; we obtained excellent agreement between our findings and the corresponding experiments.[29]

Through further modifications of the gLSM, we simulated the dynamics of photo-responsive gels, which encompass chromophores that undergo a light-induced isomerization reaction.[30–32] Additional modifications of the model allowed us to capture the behavior of chemically-reactive microposts embedded in a thermo-responsive gel[33] and optimize the self-regulating behavior of the system. Recently, we augmented our 3D gLSM to take into account the finite extensibility of the chains within gels containing loops[5]. We now adapt the latter model to account for the dynamic (temporary) binding of dangling chains.

The gLSM is based on the two-fluid model for polymer networks.[34–36] The dynamics of the polymer network is assumed to be purely relaxational, so that the forces acting on the swollen, deformed gel are balanced by the frictional drag due to the motion of the solvent. It is also assumed that the gel motion occurs solely due to the polymer-solvent interdiffusion. Hence, the velocity of the polymer, $\mathbf{v}^{(p)}$, can be calculated as [17]

$$\mathbf{v}^{(p)} = \Lambda_0(\phi/\phi_0)^{-3/2}(1-\phi)\nabla\cdot\hat{\boldsymbol{\sigma}} \ , \tag{25}$$

where Λ_0 is the kinetic coefficient, which is inversely proportional to the polymer-solvent friction coefficient η_0. In the computer simulations, we choose some l_0 and t_0 for the respective

units of length and time, and stress is measured in the units of k_BT / v_0, where v_0 is the volume of a monomeric unit within a polymer chain. Then, the kinetic coefficient Λ_0 is dimensionless and calculated as [17] $\Lambda_0 = k_BT(v_0\eta_0 l_0^2 t_0^{-1})^{-1}$.

Within the framework of the gLSM, a 3D gel sample is represented by a set of lineal hexahedral elements.[37,38] Initially, the sample is undeformed and consists of $(L_x-1)\times(L_y-1)\times(L_z-1)$ identical cubic elements; here L_i is the number of nodes in the i-direction, $i = x, y, z$. In the un-deformed state, each element is characterized by the same volume fraction ϕ_0 and cross-link density c_0. (It is worth recalling that by definition, the cross-link density is equal to the concentration of elastically active subchains in the network.) Upon deformation, the elements move together with the polymer network so that the amount of polymer and number of cross-links within each hexahedral element remain equal to their initial values. Correspondingly, the volume fraction of polymer in the element $\mathbf{m} \equiv (i, j, k)$ is determined as $\phi(\mathbf{m}) = \phi_0\Delta^3 / V(\mathbf{m})$, where Δ and $V(\mathbf{m})$ are the un-deformed element size and volume of the deformed element, respectively.

The gel dynamics is described through the motion of the nodes of the elements caused by forces acting on these nodes. After specifying the energy density $u(I_1, I_3)$, eq. (11), we use the finite element approximation (FEA) to determine the element energy density $u(\mathbf{m})$ as described in ref.[18] As a result, we obtain the total energy of the gel as

$$U_{tot} = \Delta^3 \sum_{\mathbf{m}} u(\mathbf{m}) \quad , \tag{26}$$

where the contribution from the element $\mathbf{m}$, $u(\mathbf{m})$, depends only on the coordinates of the nodes of this element denoted as $\boldsymbol{x}_n(\mathbf{m})$, $n = 1, 2, ..., 8$. (Note that $u(\mathbf{m})$ is the gel energy per unit volume of the un-deformed element.) Then, the force acting on each node is given by the equation

$$\mathbf{F}_n(\mathbf{m}) = -\frac{\partial U_{tot}}{\partial \boldsymbol{x}_n(\mathbf{m})} \quad . \tag{27}$$

The same node can belong to several elements, so the right hand side of the above equation contains contributions from all elements adjacent to a given node. Finally, the velocity of the node is proportional to the force and is determined from an equation similar to eq. (25)

$$\frac{d\boldsymbol{x}_n(\mathbf{m})}{dt} = M_n(\mathbf{m})\mathbf{F}_n(\mathbf{m}) \quad , \tag{28}$$

where $M_n(\mathbf{m})$ is the mobility of the node proportional to the kinetic coefficient Λ_0.

The contributions to $u(\mathbf{m})$ and $\mathbf{F}_n(\mathbf{m})$ due to the elastic energy of the permanent network and the polymer solvent interactions, i.e., the first three terms on the r.h.s. of eq. (11), and the mobility $M_n(\mathbf{m})$ are calculated as described in detail in ref. 17. Below, we focus solely on applying the FEA to the last term on the r.h.s. of eq. (11), $u^*_{\mathrm{el}}(t)$, that then gives the contribution of the temporary cross-links to the nodal forces.

Here, we focus on the state of equilibrium swelling of a gel that contains both cryptic bonds and dangling binding chains.

D. Model parameters and verification of the computational approach

We use the known experimental values that characterize poly(N-isopropylacrylamide) (pNIPAAm) gel.[39] Correspondingly, the polymer-solvent interaction is taken to be $\chi(\phi,T) = \chi_0(T) + \chi_1\phi$, where $\chi_0(T) = h(T_0+T)^{-1} - s$ with $h = -902.44$, $s = 3.4163$, $T_0 = 273.15$, and $\chi_1 = 0.518$.[39] The subchains between the cross-links contain $n+l$ Kuhn segments with $n = 4$ and $l = 8$, and the dangling chains contain $m = 2$ Kuhn segments (see Fig. 1). The volume fraction of polymer under the conditions of fabrication is taken to be $\phi_0 = 0.129$, and the corresponding cross-link density is determined according to eq. (8) $c_0 v_0 = \phi_0 a_0 b^{-1}(n+l+m)^{-1} = 1.84\times10^{-3}$

with the size of a monomeric unit $a_0 = 2\text{Å}$ and the Kuhn length $b = 10\text{Å}$.[40] Note that the above value of cross-link density is greater than the critical value of $c_0^* v_0 = a_0^3 b^{-3} (n+l)^{-3/2} \approx 1.92 \times 10^{-4}$ when the non-cross-linked subchains in solution start to overlap. As ϕ_0 and c_0 are related through eq. (8),this choice of $c_0 \geq c_0^*$ ensures that the polymer network is cross-linked. The dimensionless kinetic coefficient was chosen to be $\Lambda_0 = 100$.[18] In our gLSM simulations, the dimensionless units of time and length correspond to ~1s and ~40 μm, respectively, for the given choice of parameters.[16–18]

The rate constant of folding relative to that of bond rupture at zero force was taken $k_f^{(0)} / k_r^{(0)} = 200$. As the rate of folding is significantly greater than the rate of rupture, the loops have a higher probability of being folded. The rate constant for bond rupture was assumed to be equal to the rate constant for unbinding, $k_r^{(0)} / k_{uB}^{(0)} = 1$. This assumption implies that the probability for the rate of rupture in both the loops and the reactive ends of the dangling chains are similar. Further, the ratio of the rate constant of complex formation and that of the unbinding at zero force was set to $K_0 / k_{uB}^{(0)} = 2 \times 10^4$. The latter implies that the dangling chain ends have a higher probability of being bound to the unfolded loops than being detached from them. The above values were chosen to highlight the difference between the case where the unfolded loops can bind to the reactive ends and the case where the ends of the dangling chains are non-reactive and hence, the gel does not undergo the comparable binding interactions.

The force sensitivity parameters for the rate constants of bond rupture and unbinding were set to $\gamma_{0R} = 1.5$ and $\gamma_{0uB} = 0.75$, respectively. We note that in experiment, the force sensitivity could be altered by using an appropriate chemical modification.[11] The weakly interacting labile bonds in our system could be moieties containing thiol or disulfide units leading to thiol/disulfide

exchange reaction[41–44] or hydrogen bonds[45] or metallo-supramolecular bonds formed by metal ligand coordination.[46] Also, there are synthetic modular polymers that exhibit reversible unfolding due to non-covalent bonds between monomers.[47–49]

For affine deformations, the degree of swelling (λ in Fig. 2) is equal to the chain extension, so the same notation is used for the both values. The degree of gel swelling λ is defined as the lateral extension of the gel sample i.e., $\lambda = l / l_0$ where l is the length of the gel sample along the specified direction and l_0 is the length of the reference gel. We simulate the equilibrium swelling of a pNIPAAm gel as a function of temperature for the case where: (1) binding is prohibited, and (2) binding is allowed in the absence and presence of force.

First, we carried out the gLSM simulations with $1\times1\times1$ grid elements (samples that are approximately 40 μm on a side). The time step used in the gLSM simulation is $\Delta t = 0.001$. To verify the gLSM approach, in Figs. 3 and 5, we compare the results of the gLSM simulations with numerical solutions of the constitutive equation (see below). The agreement between the output from the gLSM simulations and the numerical solutions in both plots validates our computational approach. Then, we model the deformation of a gel sample of $11\times3\times5$ elements in size under action of a constant tensile force applied at one end of the sample while the other end is held fixed. Starting from the undeformed state, we show that the probability of binding p_B in a gel element could depend on the element position within the sample due to non-uniformity of the deformation.

III. Results and Discussion

We first consider an ideal scenario where at a given temperature T, a cube-shaped gel of size h_0 experiences a constant, externally applied tensile force F_g. We assume that the force is applied along the X axis. In this case, the strain tensor is diagonal and is expressed as

$$\hat{\mathbf{B}} = \begin{bmatrix} \lambda^2 & 0 & 0 \\ 0 & \lambda_\perp^2 & 0 \\ 0 & 0 & \lambda_\perp^2 \end{bmatrix} \quad . \tag{30}$$

Here, λ and $\lambda_\perp$ are the degrees of swelling along the longitudinal and transverse directions, respectively. By balancing the forces (eqs. (20)-(24)) in the two orthogonal directions, we obtain the following equations to determine the equilibrium values of λ and $\lambda_\perp$:

$$2^{-1} c_0 v_0 \phi_0^{-1} \phi [P(\bar{\lambda})\, \lambda^2 - 2^{-1} P_0(\bar{\lambda}) + p_B \zeta_0(m)] - \pi_{\mathrm{FH}}(\phi) = (h_0 \lambda_\perp)^{-2} F_g \tag{31}$$

$$2^{-1} c_0 v_0 \phi_0^{-1} \phi [P(\bar{\lambda})\, \lambda_\perp^2 - 2^{-1} P_0(\bar{\lambda}) + p_B \zeta_0(m)] - \pi_{\mathrm{FH}}(\phi) = 0 \tag{32}$$

The functions P and P_0 depend on the average chain extension $\bar{\lambda} = \sqrt{(\lambda^2 + 2\lambda_\perp^2)/3}$, and are defined as:

$$P(\bar{\lambda}) = p_U(\bar{\lambda}) \zeta(\bar{\lambda} n^{1/2} (n+l)^{-1}) + [1 - p_U(\bar{\lambda})] \zeta(\bar{\lambda}\, n^{-1/2}) + \zeta(\bar{\lambda} (n+l)^{-1/2})$$

$$P_0(\bar{\lambda}) = \zeta_0(n+l) + \zeta_0(n) \ .$$

Here, p_U and p_B as functions of $\bar{\lambda}$ are the solutions of eqs. (1) and (2) in the steady state, namely,

$$k_r\, p_U (1 - p_U) - k_f\, (p_U - p_B)^2 = 0 \quad , \tag{33}$$

$$\phi_0^{-1} \phi\, c_0\, K_{compl}(\phi)(p_U - p_B)(1 - p_B) - K_{uB}(\bar{\lambda}) p_B = 0 \quad , \tag{34}$$

and the functions $\zeta(x)$ and $\zeta_0(n)$ are given in Section II. In eqs. (31)-(34), the volume fraction of polymer ϕ depends λ and $\lambda_\perp$ because $\phi = \phi_0 \lambda^{-1} \lambda_\perp^{-2}$. The respective reaction rate constants of rupture and formation of the labile bond between two ends of a loop, k_r and k_f, are functions of the average chain extension $\bar{\lambda}$ and thus depend on λ and $\lambda_\perp$ (see Section IIA). (In the absence of the applied force, $F_g = 0$, this scenario reduces to an isotropic swelling of the gel where $\lambda = \lambda_\perp$.)

Figure 2 shows the numerical solutions of eqs. (33) and (34) for the probability of unfolding the loop, p_U, and that of binding between the exposed sites and the reactive ends of the dangling chains, p_B, as functions of the degree of gel swelling, λ, at no applied force ($F_g = 0$). For an isotropically swollen gel, $\bar{\lambda} = \lambda$ and $\phi = \phi_0 \lambda^{-3}$. Note that at a given λ, eqs. (33) and (34) describe the dynamic equilibrium between folding/unfolding of the loops and binding/unbinding of the dangling chains.

As seen in Fig. 2, the probability of unfolding a loop, p_U, is about 0.9 in the un-deformed gel ($\lambda = 1$), and remains close to 1 for the entire range of $0.6 \le \lambda \le 2$ considered here. For the range $0.6 < \lambda < 1$, the sample is under isotropic compression, leading to an increase in ϕ. The probability of binding between an exposed site and a reactive end, p_B, is relatively high in this range due to the increase in the rate of complex formation, K_{compl}, with the increase in ϕ (see eq. (9)). (Note that the rate constant for complexation is 2×10^4 higher than the rate of breaking the bonds between the loops and reactive ends.) Under compression, the probably of unfolding the loops is still rather high (see Fig. 2) because the binding of the dangling chains to the exposed cryptic sites inhibits the folding of the loops (see eqs. (1) and (33)).

With the relative decrease in compression (as λ approaches 1), p_U shows a slight decrease because the isotropic expansion of the gel at $\lambda \sim 1$ is not large enough to unfold more loops, but the decrease in p_B with an increase in λ permits some loops to refold.

Beyond $\lambda = 1.0$, the gel is swollen and the strain induced by the swelling causes loops to unfold, as evidenced by the increase in p_U. Most of the temporary cross-links are broken by the increase in strain and hence, the binding probability progressively decreases.

A. Effect of varying temperature

We first determine the behavior of the system in the absence of an applied force. Recall that the gel exhibits LCST behavior and thus swells as the temperature is lowered. To gain insight into the behavior of this system, we plot the equilibrium degree of gel swelling as a function of temperature (Fig. 3). Using the gLSM, we determine λ for the equilibrated gels in the temperature range $T = 15°\text{C}$ to $T = 45°\text{C}$. The gels are $1 \times 1 \times 1$ units in size, corresponding to samples that are $40\,\mu\text{m}$ on each side. We consider two different scenarios: (1) the ends of the dangling chains are treated as inert and cannot participate in binding and (2) the ends of the dangling chains are reactive and can bind to sites that are exposed as the loops unfold. For scenario (1), we use $K_0 = 0$ and $\gamma_{0uB} = 0$ in the simulations. The rest of the parameters are the same for the both scenarios.

One significant difference between the cases involving binding (red) and no binding (green) (Fig. 3) is a shift in the volume phase transition temperature, T_c, to lower values when binding is present. Another apparent difference between the binding and no binding cases is that the binding interactions (red curves) lead to a decrease in the lateral extension of the gel relative to the solid green curve (no binding). Both the shift in the volume phase transition temperature and the reduction in the gel size near T_c are due to the presence of the temporary cross-links between the exposed cryptic sites (on the opened loops) and the reactive dangling ends. These cross-links act as "struts" that inhibit the swelling of the gel. In effect, the struts increase the stiffness of the network and thus, the gel undergoes a self-stiffening in response to the decrease in temperature.

Below T_c, the swelling of the LCST gel leads to a buildup in the internal force acting on the loops (even in the absence of applied force). The dangling chains that are bound to the exposed cryptic sites experience the force due to the swelling of the gel and the rupture rate between a dangling end and cryptic site increases. As the temperature is lowered well below T_c (Fig. 3), the

temporary cross-links gradually rupture and hence, the difference between the red (binding allowed) and green (no binding) lines diminishes.

These changes in the internal structure of the gel are reflected in the behavior of the probability of unfolding, p_U, and the probability of binding, p_B, with variations in temperature, as shown in Fig. 4. When the ends are reactive and complexation can occur (Fig 4a), p_B decreases, and concomitantly p_U slightly increases with lowering temperature just below T_c, thus indicating smooth variations in the number of temporary cross-links between the exposed cryptic sites and dangling ends. These temporary cross-links reduce the effect of the swelling-induced internal strain and hence act as a restoring force. On the other hand, when the ends of the dangling chains are non-reactive (i.e., binding is prohibited and does not inhibit folding of the loops), the internal strain due to gel swelling is sufficiently large to unfold the loops, as indicated by a relatively steep increase in p_U just below T_c (Fig. 4b).

Figure 4 also confirms that when the temperature is decreased further below T_c, the temporary cross-links are broken by the increasing internal strain as indicated by the monotonic decrease in the value of p_B. Additionally, the internal strain due to gel swelling causes the loops to unfold, as seen by the gradual increase in p_U.

Near T_c, the complexation leads to ~18% decrease in the degree of swelling of the gel as compared to the no binding case (Fig. 3). In other words, the formation of the temporary cross-links leads to the self-stiffening behavior.

As the temperature is increased above T_c, the difference between the green (no binding) and red (binding) curves in Fig 3 diminishes. Above T_c, the gel behavior changes from hydrophilic to hydrophobic. The polymer network expels the solvent and the gel stays relatively collapsed so

that $\lambda < 1$. (The free dangling chains undergo a coil-globule transition and thus are also effectively collapsed). In the theoretical model, the molecular interaction governing the phase transition is captured through the empirical parameter $\chi : \chi(\phi, T)$ in the Flory-Huggins term,[39] which depends on the volume fraction of the polymer network, ϕ and the temperature T. The volume fraction of the polymer in the as-prepared gel network is the same in both the scenarios i.e., binding and no binding. In this temperature range, although ~40% of the dangling chains remain bound to the open cryptic sites (Fig. 4a), binding has little effect on the volume of the gel because the value of ϕ is nearly the same for both binding and no binding cases. Additionally, we checked the swelling curve for a corresponding gel that does not undergo internal restructuring i.e., at zero probabilities of both loop unfolding and chain binding (not shown here). The example of $p_U = 0$ and $p_B = 0$ is a limiting case for the scenario where binding is not allowed. The zero probability of unfolding does not allow the gel to swell as temperature is decreased below the LCST and thus leads to a smaller degree of swelling as compared to the gel system where folding-unfolding is allowed but binding is not allowed (see green curve in Fig. 3).

B. Effect of applying a constant force.

In the cases considered above, the binding of the dangling chains to the exposed cryptic sites shows a pronounced effect on gel swelling for the chosen values of the reaction rate constants and chain segment lengths. The internal force due to swelling was sufficiently strong to unfold only a fraction of the loops (see Figs. 4a and 4b). We demonstrate below that the introduction of an applied force amplifies the differences between the cases involving binding and no binding. For

this discussion, it is convenient to introduce the dimensionless force as $F = F_g / F_0$, where $F_0 = c_0 v_0 h_0^2$ is the unit of force. Figure 5 shows how λ and $\lambda_\perp$, i.e., the extensions of the sample along and normal to the direction of force, respectively, vary with temperature if a constant tensile force of $F = 3$ is applied.

In the direction of the applied force (Fig. 5a), the disparity between the binding and no binding curves for *F*=3 around and below T_c is even smaller than that for the $F = 0$ situation. The external force amplifies the effects of the internal strain due to the gel swelling and thus, the probability of unfolding, p_U, is increased. Consequently, with an applied force of *F*=3, the system encompasses a greater fraction of unbound temporary cross-links than the $F = 0$ case.

In the direction transverse to the force, however, the gel is compressed as $\lambda_\perp \le 1$ (Fig. 5b). At $T \approx 33^{\circ}\mathrm{C}$, the sample with binding is compressed by 50% more than the case where the formation of the transient cross-links is not allowed (Fig. 5b). As the sample becomes compressed in the transverse direction, the reactive ends are brought closer to any exposed cryptic sites and thus, the dangling chains and unfolded loops can form temporary cross-links.

Figure 5 shows that in the presence of the temporary cross-links, the LCST temperature is shifted to $\sim 33^{\circ}\mathrm{C}$ from that of $\sim 35.5^{\circ}\mathrm{C}$, when no binding of the dangling chains is allowed. This results in a notable difference in the sizes of the gels with and without the temporary cross-links within the temperature range from $\sim 33^{\circ}\mathrm{C}$ to $\sim 35.5^{\circ}\mathrm{C}$ as seen in Fig. 5.

The red curves in Fig. 5 shows that under deformation, the gel contracts by 3.2% in the lateral direction (Fig. 5a) and by 50% in the transverse direction (Fig 5b) when binding is permitted. In the latter scenario, essentially all the loops in the gel are unfolded at all temperatures, and a significant fraction of the unfolded loops are bound to the reactive ends for $T > T_c$. (see Fig.

6a). (To highlight the effects of the applied force on the binding interactions, the behavior of the system with no binding is shown in Fig. 6b.) As the applied force is sufficiently strong to unfold all the loops, the relative value of contraction is relatively low in the direction of force (red curve in Fig. 5a), and high in the direction normal to the force (red curve in Fig. 5b).

At T < T_c , Fig. 6a shows a monotonic decrease in the value of p_B with decreasing temperature, and helps explain the convergence of the red (binding) and the green (no binding) curves as T is decreased (Fig. 5). The decrease in p_B indicates a decrease in the self-stiffening effect when an external force is applied. Namely, the external force ruptures the temporary cross-links that give rise to the self-stiffening. And hence, the red and green curves show a smaller difference near the transition temperature.

To summarize, for the $F = 0$ case, the system displays a roughly 18% decrease in the lateral extension of the gel (at $T \approx 31.5^{o}$ C) when the binding is present. For the $F = 3$ case, the gel displays only roughly 3 % decrease (at $T \approx 33^{o}$ C) in λ along the stretching direction, and 50 % decrease $\lambda_{\perp}$ perpendicular to the stretching direction when the binding is present.

The above calculations reveal the behavior of the gel at steady state. Using the gLSM, we can analyze the dynamic response of the gel as the sample approaches the steady state configuration in the presence of a constant applied force (Fig. 7). Moreover, the gLSM simulations allow us to simulate the behavior of relatively large samples. In particular, we consider a gel that is $11\times3\times5$ elements in size and is structurally uniform, i.e., all gel elements have the same molecular structure in the un-deformed state. As shown in Fig. 7a, all the nodes at the left most end of the gel are held fixed, and a constant tensile force F is applied along the entire face at the opposite end of the sample. In the simulations, we take $F = 50$ so the force per node is ~2.08 as

there are twenty four nodes on the end surface. For comparison, the force per node is 0.75 in the gLSM simulations of a single gel element (Figs. 5 and 6).

In the current simulations, we assume that the temporary crosslinks form and break fast enough that the contribution of the temporary crosslinks to the stress tensor can be described by the steady state equation, eq. (24). This assumption leads to a simplification of the simulations because the memory effects described by eq. (23) are neglected. Specifically, after each step of the gLSM simulation, we determine $\bar{\lambda}$ for each element, update the local values of p_U and p_B by solving numerically eqs. (33) and (34), and then apply eq. (24).

The simulation results in Fig. 7 demonstrate that the application of force results in a non-uniform gel structure. The non-uniform deformation of the sample is seen to result in a variation of the volume fraction of polymer and number of temporary cross-links within the initially uniform gel sample (Fig. 7). Figure 7 shows that the elements nearer to the right surface (where the force is applied) experience a greater strain when the sample is stretched. This strain leads to breakage of the temporary cross-links, as indicated by the decrease in the probability of binding from the right to the left side of the sample (Fig. 7).

With an increase in time (Fig. 7b-d), the strain on the left end of the gel also contributes to a decrease in p_B in the nearby elements. Finally, the sample equilibrates at the given force, as evidenced by the symmetry in the probability of binding in the gel elements (see Fig. 7d).

IV. Conclusions

To harness the utility of bio-inspired cryptic bonds within gels, we designed polymer networks encompassing sites that are exposed under mechanical deformation and can subsequently bind to reactive groups on dangling chains, which are ever-present in polymer gels. Through models developed here, we showed that these temporary cross-links effectively reinforce the

material so that it resists swelling as the temperature is reduced (Fig. 3) or an external force is applied to the sample (Fig. 5). These studies were primarily aimed at demonstrating a proof of concept; in future work, we will utilize our model to pinpoint regions in parameter space where the binding between the exposed cryptic sites and the dangling ends provide maximal reinforcement of the system.

One of the advantageous features of this system is that the binding events are reversible. An increase in temperature or the release of the tensile deformation can lead to the breakage of the temporary cross-links and the return of the material to its original state. For instance, the initially designed state can be recovered after a critical loading event. Hence, the same system can be used or re-used for multiple applications.

Another distinct feature of the system is that its properties can be dynamically tailored through deformation. The mechanical routes to modifying the systems' behavior described here do not require high temperatures or extreme conditions, and thus, could constitute energy-efficient and cost-effective methods for processing materials.

Applied as a coating, a network that becomes self-reinforcing or self-stiffening in response to deformation can act as "dermal armor" to protect the underlying system from damage. Such responsive self-forming armor can extend the life-time of manufactured components. More generally, our findings can help advance the burgeoning field of mechano-mutable materials by providing guidelines for "co-designing" the mechano-responsive elements and the applied forces to produce the desired mechanical behavior, and for addressing the pervasive need for materials that provide a beneficial response to mechanical stress.

Conflicts of Interest

There are no conflicts of interest to declare.

Acknowledgements

ACB gratefully acknowledges financial support from DOE grant number DE-FG02-90ER45438 for the development of the theoretical model and the ARO grant number W911NF-19-1-0388-(75173-MS) for the development of the computer simulations.

References

1 E. Klotzsch, M. L. Smith, K. E. Kubow, S. Muntwyler, W. C. Little, F. Beyeler, D. Gourdon, B. J. Nelson and V. Vogel, *Proc. Natl. Acad. Sci. U. S. A.*, 2009, **106**, 18267–72.

2 F. Grinnell, *J. Cell. Biochem.*, 1984, **26**, 107–116.

3 R. Pankov and K. M. Yamada, *J. Cell Sci.*, 2002, **115**, 3861–3.

4 O. Peleg, T. Savin, G. V. Kolmakov, I. G. Salib, A. C. Balazs, M. Kröger and V. Vogel, *Biophys. J.*, 2012, **103**, 1909–1918.

5 S. Biswas, V. V Yashin and A. C. Balazs, *Soft Matter*, 2018, **14**, 3361–3371.

6 Y. H. Tran, M. J. Rasmuson, T. Emrick, J. Klier and S. R. Peyton, *Soft Matter*, 2017, **13**, 9007–9014.

7 H. Zhou, J. Woo, A. M. Cok, M. Wang, B. D. Olsen and J. A. Johnson, *Proc. Natl. Acad. Sci. U. S. A.*, 2012, **109**, 19119–24.

8 G. I. Bell, *Science*, 1978, **200**, 618–627.

9 M. Rubinstein and R. H. Colby, *Polymer Physics*, Oxford University Press, Oxford, 2003.

10 B. V. S. Iyer, V. V. Yashin, T. Kowalewski, K. Matyjaszewski and A. C. Balazs, *Polym. Chem.*, 2013, **4**, 4927–4939.

11 B. V. S. Iyer, I. G. Salib, V. V. Yashin, T. Kowalewski, K. Matyjaszewski and A. C. Balazs, *Soft Matter*, 2013, **9**, 109–121.

12 M. J. Hamer, B. V. S. Iyer, V. V. Yashin and A. C. Balazs, *Nano Lett.*, 2014, **14**, 4745–

4750.

13 M. J. Hamer, B. V. S. Iyer, V. V. Yashin, T. Kowalewski, K. Matyjaszewski and A. C. Balazs, *Soft Matter*, 2014, **10**, 1374–1383.

14 B. V. S. Iyer, V. V. Yashin, M. J. Hamer, T. Kowalewski, K. Matyjaszewski and A. C. Balazs, *Prog. Polym. Sci.*, 2015, **40**, 121–137.

15 K. Ito, J. Chuang, C. Alvarez-Lorenzo, T. Watanabe, N. Ando and A. Y. Grosberg, *Prog. Polym. Sci.*, 2003, **28**, 1489–1515.

16 V. V. Yashin and A. C. Balazs, *Science*, 2006, **314**, 798–801.

17 V. V. Yashin and A. C. Balazs, *J. Chem. Phys.*, 2007, **126**, 124707.

18 O. Kuksenok, V. V. Yashin and A. C. Balazs, *Phys. Rev. E - Stat. Nonlinear, Soft Matter Phys.*, 2008, **78**, 041406.

19 L. Anand, *Comput. Mech.*, 1996, **18**, 339–355.

20 P. J. Flory, *Trans. Faraday Soc.*, 1960, **56**, 722–743.

21 A. D. Drozdov, *Finite Elasticity and Viscoelasticity*, World Scientific, Singapore, 1996.

22 V. V. Yashin, O. Kuksenok and A. C. Balazs, *Prog. Polym. Sci.*, 2010, **35**, 155–173.

23 V. V. Yashin, O. Kuksenok, P. Dayal and A. C. Balazs, *Reports Prog. Phys.*, 2012, **75**, 066601.

24 O. Kuksenok, V. V. Yashin and A. C. Balazs, *Soft Matter*, 2009, **5**, 1835–1839.

25 V. V. Yashin, K. J. Van Vliet and A. C. Balazs, *Phys. Rev. E*, 2009, **79**, 046214.

26 V. V. Yashin, O. Kuksenok and A. C. Balazs, *J. Phys. Chem. B*, 2010, **114**, 6316–22.

27 I. C. Chen, O. Kuksenok, V. V. Yashin, A. C. Balazs and K. J. Van Vliet, *Adv. Funct. Mater.*, 2012, **22**, 2535–2541.

28 T. Ueno, K. Bundo, Y. Akagi, T. Sakai and R. Yoshida, *Soft Matter*, 2010, **6**, 6072–6074.

29 P. Yuan, O. Kuksenok, D. E. Gross, A. C. Balazs, J. S. Moore and R. G. Nuzzo, *Soft Matter*, 2013, **9**, 1231–1243.

30 O. Kuksenok and A. C. Balazs, *Adv. Funct. Mater.*, 2013, **23**, 4601–4610.

31 O. Kuksenok and A. C. Balazs, *Sci. Rep.*, 2015, **5**, 9569.

32 O. Kuksenok and A. C. Balazs, *Mater. Horiz.*, 2016, **3**, 53–62.

33 X. He, M. Aizenberg, O. Kuksenok, L. D. Zarzar, A. Shastri, A. C. Balazs and J. Aizenberg, *Nature*, 2012, **487**, 214–218.

34 B. Barrière and L. Leibler, *J. Polym. Sci. Part B Polym. Phys.*, 2003, **41**, 166–182.

35 A. Onuki, *Adv. Polym. Sci.*, 1993, **109**, 63–121.

36 M. Doi, *J. Phys. Soc. Japan*, 2009, **78**, 052001.

37 I. M. Smith, D. V. Griffiths and L. Margetts, *Programming the Finite Element Method*, John Wiley & Sons, 2013.

38 O. C. Zienkiewicz, R. L. Taylor and J. Z. Zhu, *The Finite Element Method: Its Basis and Fundamentals*, Butterworth-Heinemann, 7th edn., 2013.

39 S. Hirotsu, *J. Chem. Phys.*, 1991, **94**, 3949.

40 D. Magerl, M. Philipp, E. Metwalli, P. Gutfreund, X.-P. Qiu, F. M. Winnik and P. Müller-Buschbaum, *ACS Macro Lett.*, 2015, **4**, 1362–1365.

41 J. K. Oh, C. Tang, H. Gao, N. V. Tsarevsky and K. Matyjaszewski, *J. Am. Chem. Soc.*, 2006, **128**, 5578–5584.

42 K. Min, H. Gao, J. A. Yoon, W. Wu, T. Kowalewski and K. Matyjaszewski, *Macromolecules*, 2009, **42**, 1597–1603.

43 J. K. Oh, R. Drumright, D. J. Siegwart and K. Matyjaszewski, *Prog. Polym. Sci.*, 2008, **33**, 448–477.

44 N. V. Tsarevsky, K. Min, N. M. Jahed, H. Gao and K. Matyjaszewski, in *ACS Symposium Series*, 2006, vol. 939, pp. 184–200.

45 P. Cordier, F. Tournilhac, C. Soulié-Ziakovic and L. Leibler, *Nature*, 2008, **451**, 977–980.

46 M. Ahmadi and S. Seiffert, *Soft Matter*, 2020, **16**, 2332–2341.

47 J. T. Roland and Z. Guan, *J. Am. Chem. Soc.*, 2004, **126**, 14328–14329.

48 Z. Guan, J. T. Roland, J. Z. Bai, S. X. Ma, T. M. McIntire and M. Nguyen, *J. Am. Chem. Soc.*, 2004, **126**, 2058–2065.

49 J. Chung, A. M. Kushner, A. C. Weisman and Z. Guan, *Nat. Mater.*, 2014, **13**, 1055–1062.

Figure Captions

Fig. 1 (top) Schematic of a polymer gel network containing loops in folded and unfolded state, and dangling chains with reactive ends. Polymer network is represented in green. Grey solid circles represent cross-links and the reactive labile bonds are shown in blue when bonded and forms a loop, and in red when the labile bonds of the loop are broken or when they form bonds with reactive ends of the dangling chains shown in yellow. The bottom panel displays a magnified representation of the chains with n Kuhn segments containing loops with l Kuhn segments in folded (left) and unfolded state (center). The dangling chains contains m Kuhn segments and are shown as bound to the exposed cryptic bonds (right).

Fig. 2 The probability of unfolding of the loop, p_U, and probability of binding of the dangling chains, p_B, in the steady-state as functions of the chain extension, λ. The model parameter values are given in the text. The lines denote the numerical solution of the steady state equations, eqs.

(33) and (34), obtained using *Mathematica*™. The symbols denote the numerical solution of the rate equations, eq. (1) and (2), in the long time limit obtained by the ODE solver used as a part of the gLSM code. Comparison of the two solutions serves as a partial verification of the gLSM code.

Fig. 3 The lateral extension of the gel λ at the steady-state as a function of temperature T for the cases of binding allowed (red) and binding not allowed (green). Note that the difference in the degree of swelling between the two cases is greater near the transition temperature. The model parameter values are given in the text. The lines show the numerical solution of eq. (31) at $F_g = 0$ and $\lambda = \lambda_\perp$ obtained using *Mathematica*™. The symbols show the numerical solution obtained using the gLSM code applied for a single gel element in the long time limit. Comparison of the two solutions serves as a partial verification of the gLSM code.

Fig. 4 The probability of unfolding of a loop, p_U, and probability of binding of a dangling chain, p_B, in the steady-state as functions of temperature T for the cases of binding (a) allowed and (b) not allowed. The model parameter values are given in the text. The notations are the same as in Fig. (2).

Fig. 5 (a) The lateral, λ, and (b) transverse, $\lambda_\perp$, extensions of the gel under the action of applied tensile force of $F = 3$ in the steady state as functions of temperature T for the cases of binding allowed (red) and not allowed (green). Application of the tensile force results in the lateral extension greater than that in the absence of force (see Fig. 3). Note that the difference in swelling between the two cases is greater near transition temperature. The model parameter values are given in the text. The lines show the numerical solution of eq. (31)-(34) obtained using *Mathematica*™.

The symbols show the numerical solution obtained using the gLSM code applied for a single gel element in the long time limit. Comparison of the two solutions serves as a partial verification of the gLSM code.

Fig. 6 The probability of unfolding of a loop, p_U, and probability of binding of a dangling chain, p_B, under the action of applied tensile force of $F = 3$ in the steady-state as functions of temperature T for the cases of binding (a) allowed and (b) not allowed. Note that the applied force is large enough to result in unfolding all the loops as indicated by $p_U \approx 1$. The model parameter values are given in the text. The notations are the same as in Fig. (2).

Fig. 7 The effect of a tensile force on a gel sample of dimension $11 \times 5 \times 3$ at $T = 30°\text{C}$. Coloring represents the probability of binding, p_B, in each gel element. The force of $F = 50$ is applied to the right end of the gel sample, and the left end is fixed to a solid wall. Panel (a) shows the initial gel sample. Panels (b) and (c) show the gel sample after the respective 10^4 and 3×10^4 time steps of the gLSM simulations. Panel (d) shows the final stationary configuration attained by the gel sample under the applied constant force. It is assumed that the temporary crosslinks form and break fast enough to neglect the memory effects (see the text). The model parameter values are given in the text.

Figure 1

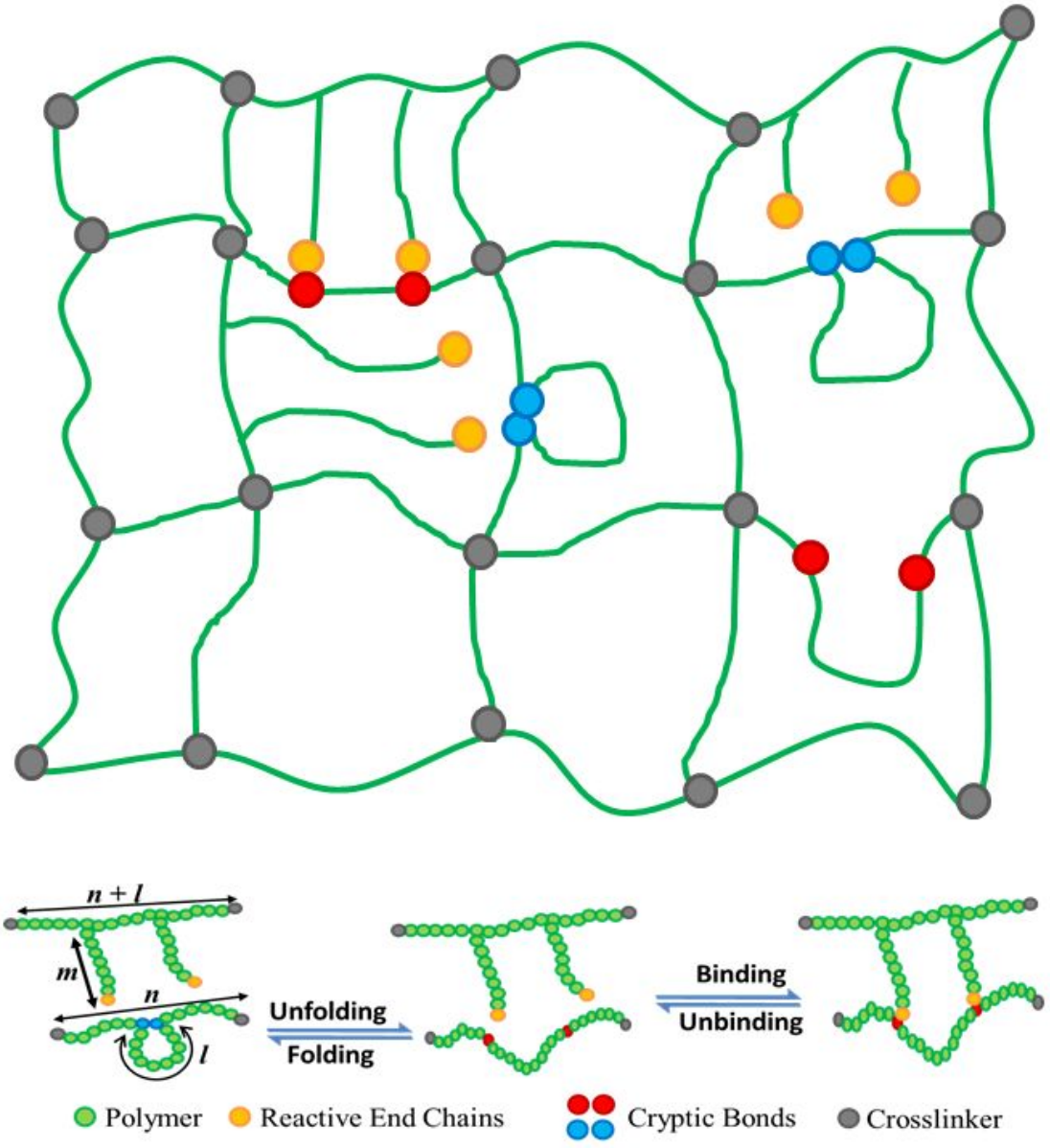
n + l
m
n
l
Unfolding
Folding
Binding
Unbinding
Polymer
Reactive End Chains
Cryptic Bonds
Crosslinker

Figure 2

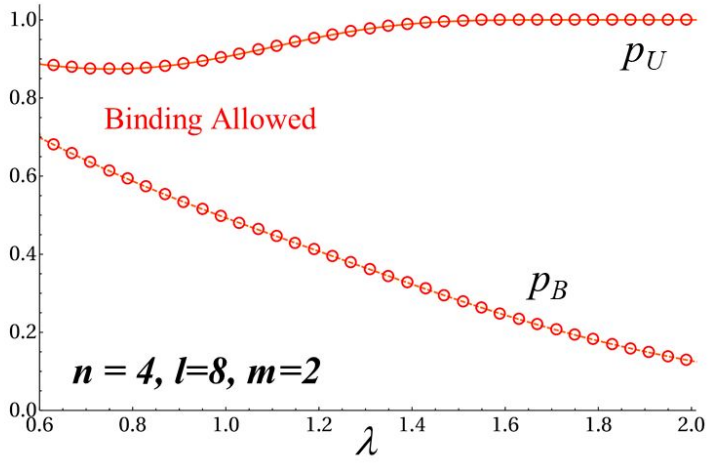
1.0
0.8
0.6
0.4
0.2
0.0
0.6
0.8
1.0
1.2
1.4
1.6
1.8
2.0
λ
p_U
Binding Allowed
p_B
n = 4, l=8, m=2

Figure 3

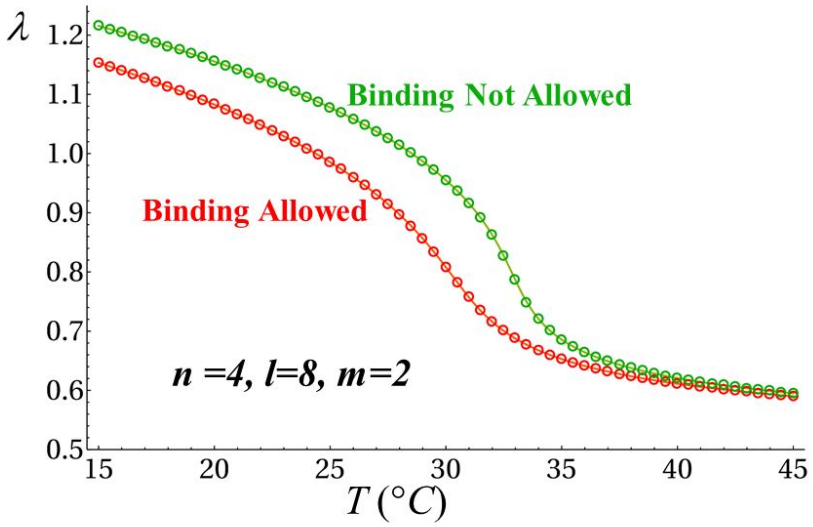
λ
1.2
1.1
1.0
0.9
0.8
0.7
0.6
0.5
Binding Not Allowed
Binding Allowed
n =4, l=8, m=2
15
20
25
30
35
40
45
T (°C)

Figure 4

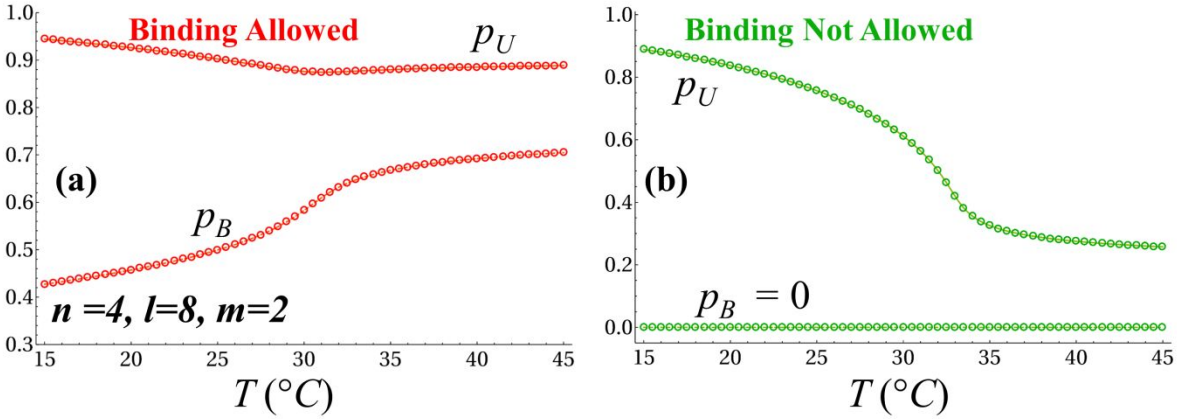
Binding Allowed
p_U
(a)
p_B
n =4, l=8, m=2
$T\,(°C)$
Binding Not Allowed
p_U
(b)
$p_B = 0$
$T\,(°C)$

Figure 5

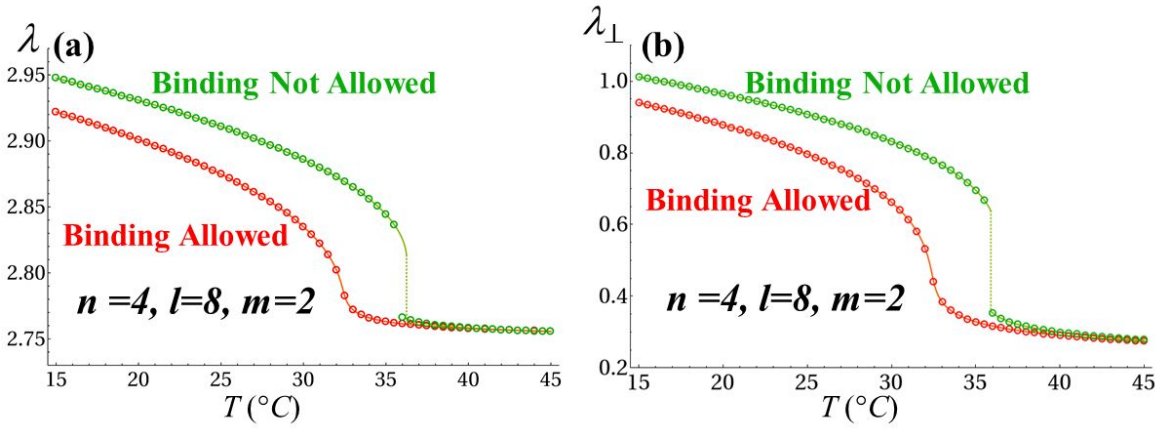
λ
(a)
Binding Not Allowed
Binding Allowed
n =4, l=8, m=2
2.95
2.90
2.85
2.80
2.75
15
20
25
30
35
40
45
T (°C)
λ⊥
(b)
Binding Not Allowed
Binding Allowed
n =4, l=8, m=2
1.0
0.8
0.6
0.4
0.2
15
20
25
30
35
40
45
T (°C)

Figure 6

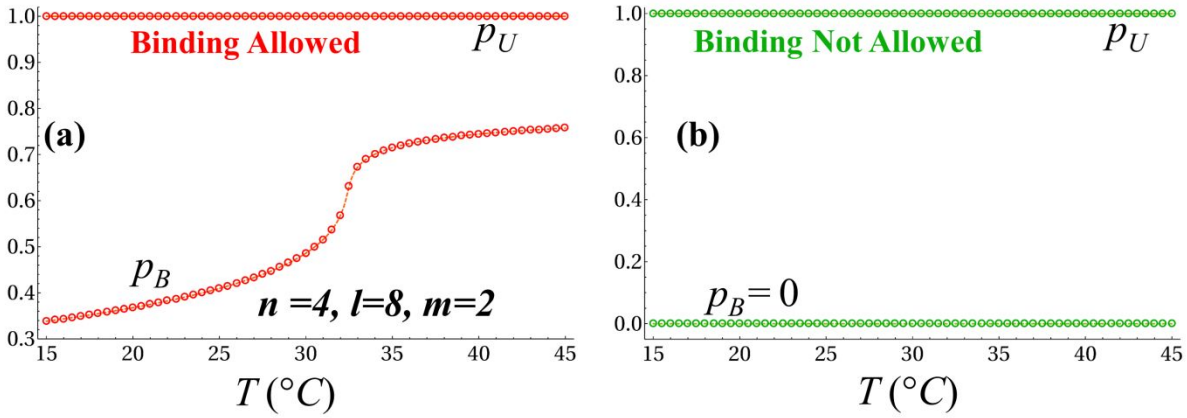
Binding Allowed
p_U
(a)
p_B
n =4, l=8, m=2
$T\,(°C)$
Binding Not Allowed
p_U
(b)
$p_B = 0$
$T\,(°C)$

Figure 7